World Scientific Publishing Co Pte Ltd

Postal & Correspondence:
Farrer Road
P O Box 128
Singapore 912805

Office:
5 Toh Tuck Link
Singapore 596224
Tel: (65) 6466 5775 Fax: (65) 6467 7667

E-mail: wspc@wspc.com.sg
http://www.worldscientific.com/

URGENT IJBC PROOFS

Please check these proofs immediately and return the corrected set by express air/email to Journals Department (IJBC), World Scientific Publishing Co Pte Ltd, 5 Toh Tuck Link, Singapore 596224.

Date: 10 April 2014

Paper title: An Intrinsically Three-Dimensional Fractal

Author(s): M. Fernandez-Guasti

To appear in International Journal of Bifurcation and Chaos, Vol. 24 No. 6.

Dear Author,

Enclosed are the proofs of your paper for you to correct printer's errors, if any. Please do not improve or update your paper at this stage, as this is expensive and causes delays.

Thank you.

Yours sincerely

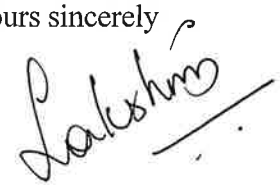

Lakshmi Narayan (Ms)
Journal Dept.
(IJBC)
Email: lakshmi@wspc.com.sg

Encl.

World Scientific Publishing Co Pte Ltd
Reg. No: 198004665C

Postal & Correspondence:
Farrer Road
P O Box 128
Singapore 912805

Office:
5 Toh Tuck Link
Singapore 596224
Tel: (65) 6466 5775 Fax: (65) 6467 7667

E-mail: wspc@wspc.com.sg
http://www.worldscientific.com

To: Journal Department

INTERNATIONAL JOURNAL OF BIFURCATION AND CHAOS
(OFFPRINT ORDER FORM)

AUTHORS MAY OPT TO RECEIVE EITHER OF THE FOLLOWING:
- ❑ **10** OFFPRINTS OF EACH ARTICLE FREE OF CHARGE, **or**
- ❑ A COMPLIMENTARY PDF OF THE ARTICLE

Additional offprints are available at the prices listed in the table below:

Number of Pages	Additional Offprints Required (cost in US$)			
	50	100	150	200
1 to 4	117.19	148.38	172.25	202.75
5 to 8	195.25	244.13	294.88	341.50
9 to 12	288.13	360.13	434.50	508.38
13 to 16	373.69	449.50	542.50	629.75
17 to 20	481.88	582.38	704.75	815.50
21 to 24	561.00	673.25	819.63	944.00
25 to 28	669.13	806.50	983.25	1130.13
29 to 32	797.38	958.13	1171.25	1346.50

Prices subject to change without notice.

In addition to my **10** free copies (or complimentary pdf), I would like to order _____ copies.

Please fill in this order form and return it to us, even if you do not require any offprints, by _____.

Title of article: _____

_____

Journal: _____

Ship to:

Name: _____

Address: _____

_____

_____

_____

Fax: _____

Tel: _____

E-mail: _____

Bill to:

Name: _____

Address: _____

_____

_____

_____

Fax: _____

Tel: _____

E-mail: _____

PTO

Payment enclosed for US $ _____

Charge to my card: ❑ Visa ❑ MasterCard ❑ Amex ❑ Diners Club

Card number: _____ Expiry date: _____

All offprints will be sent by surface mail. There will be an extra charge for airmail.

Contributors can purchase a copy of the issue at US$35. Please contact: sales@wspc.com.sg

Special Request

In case your department does not subscribe to the journal:
Please provide us with the name and address of your library, so that we can inform your librarian about this journal.

_____

_____

TERMS OF DELIVERY

1. No offprints will be sent unless the order form is filled in and returned by the stipulated date.
2. Offprints will be supplied at the prices listed in the table. Any blank pages necessary to complete printer's forms will cost the same as printed pages.
3. Please ask for quotations for orders involving more than 32 pages or more than 200 copies. For orders exceeding 200 copies, please order in lots of 100.
4. Offprints ordered after an issue has gone to press will be charged substantially higher than the prices listed in the table.

An. Fig. 5 – higher resolution image available

International Journal of Bifurcation and Chaos, Vol. 24, No. 6 (2014) 1430017 (13 pages)

DOI: 10.1142/S0218127414300171

An Intrinsically Three-Dimensional Fractal

M. Fernández-Guasti
Lab. de Óptica Cuántica, Depto. de Física,
Universidad A. Metropolitana – Iztapalapa,
09340 México D.F., Ap. postal. 55-534, Mexico
mfg@xanum.uam.mx

Received ; Revised

The quadratic iteration is mapped using a nondistributive real scator algebra in three dimensions. The bound set **S** has a rich fractal-like boundary. Periodic points on the scalar axis are necessarily surrounded by off axis divergent magnitude points. There is a one-to-one correspondence of this set with the bifurcation diagram of the logistic map. The three-dimensional **S** set exhibits self-similar 3D copies of the elementary fractal along the negative scalar axis. These 3D copies correspond to the windows amid the chaotic behavior of the logistic map. Nonetheless, the two-dimensional projection becomes identical to the nonfractal quadratic iteration produced with hyperbolic numbers. Two- and three-dimensional renderings are presented to explore some of the features of this set.

Keywords: 3D bifurcations; hyper-complex numbers; 3D hyperbolic numbers; real scators; quadratic iteration; Mandelbrot set; discrete dynamical systems.

1. Introduction

Although chaotic behavior in three-dimensional dynamical systems abound, they are not so common in discrete dynamical systems. Two-dimensional fractal structures have often been extended to higher dimensions. For example, Sierpinski triangles are extended to three-dimensional tetrahedrons that produce square-based pyramids the Sierpinski carpet into the three-dimensional Menger sponge, sphere inversion fractals as a generalization of circle inversion [Leys, 2005], Mandelbulb [Rama & Mishra, 2011], Mandelbox and several other approaches to generalizations of fractals in the complex plane to three or four dimensions. However, these extensions do not always produce a higher dimensional fractal structure. Take, for example, quaternion quadratic iterations in parameter space that merely produce solids of revolution with an M-set section. The visualization of fractal geometry, even in two dimensions, is a rich subject [Blackledge, 2002]. Visualization of three-dimensional structures is even more complicated and requires elaborate time consuming algorithms [Dodge *et al.*, 2008].

It is not common practice to proceed the other way around — Namely, to produce a discrete three-dimensional fractal structure and thereafter obtain two-dimensional projections of such objects. In the present approach, the three-dimensional product and additional operations required to produce a quadratic mapping are introduced. Generalizations of hyperbolic complex ($i^2 \equiv +1$, $i \notin \mathbb{R}$) or complex ($i^2 \equiv -1$) numbers to higher dimension division algebras are severely limited by Hurwitz and Frobenius theorems. However, if divisors of zero are permitted, the scope becomes much broader. The term "scator" has been coined to describe numbers that contain a scalar and one or more director components. Hyperbolic and complex numbers or Hamilton's quaternions are early examples of this type of structures [Kantor & Solodovnikov, 1989]. Clifford algebras generalize these examples as well as many other hypercomplex number systems [Helmstetter & Micali, 2008; Sabadini *et al.*, 2009].

A number system becomes an algebra when it is endowed with two operations, usually labeled addition and product. The hyperbolic or real scator algebra [Fernández-Guasti & Zaldívar, 2013] employed here is remarkable on several grounds: On the one hand, it exhibits commutative group properties in a restricted space where divisors of zero are excluded. On the other hand, it can be implemented in an arbitrary number of dimensions. Furthermore, it is possible to establish an order parameter. However, these features are in detriment of distributivity. The scator product does not distribute over addition. Nonetheless, as we shall presently see, this restriction does not prevent the scator algebra number system from generating consistent iterated mappings. The iteration of the quadratic function with three variables is compared with an appropriate order parameter. The outcome is a bound set with a rather intricate boundary. It comes as a surprise that a three-dimensional confined set, produced with real scator algebra, exhibits fractal features whereas the two-dimensional projection does not. This projection is isomorphic to hyperbolic complex numbers, also called double numbers. Under the quadratic iteration, it is known that double numbers produce a square bound set with a smooth boundary that does not show fractal features.

The structure of this manuscript is as follows: In Sec. 2, the necessary elements of real scator algebra in $1+2$ dimensions are introduced. Emphasis is laid on the squaring function and the conditions that permit the rendering of inverse orbits. The quadratic iteration with this number system is presented in Sec. 3. In Sec. 3.1, it is shown that the three-dimensional set exhibits the same one-to-one correspondence with the period doubling bifurcation diagram of the logistic map. In Sec. 3.2, it is demonstrated that there exists a divergent magnitude surface in the vicinity of every periodic point on the scalar axis. The double numbers limit and 2D projections in the s, x plane are presented in Sec. 4. Conclusions are drawn in the last section.

2. Hyperbolic Scators

Real scator elements, also referred to as hyperbolic scators, in $1+2$ dimensions can be written in terms of three real numbers [Fernández-Guasti & Zaldívar, 2013]

$$\overset{o}{\varphi} = (s; x, y), \quad s, x, y \in \mathbb{R}.$$

The first component, named the scalar component, stands on a different footing from the rest. To stress this fact, it is separated by a semi-colon from the other components. Subsequent components, separated by commas, stand on an equal footing. They are named the director components because they possess the quality of direction. Scator elements are represented with an oval placed overhead.[1] To establish an algebra, two operations are required. The *addition* operation for scators is defined adding component by component $\overset{o}{\varphi}_a + \overset{o}{\varphi}_b = (s_a; x_a, y_a) + (s_b; x_b, y_b) = (s_a + s_b; x_a + x_b, y_a + y_b)$. The scator set forms a commutative group under the addition operation. The *product* operation of two equal hyperbolic scators, that is, the square of a hyperbolic scator $\overset{o}{\varphi} = (s; x, y)$ is defined by

$$\begin{aligned}\overset{o}{\varphi}^2 &= (s_\diamond; x_\diamond, y_\diamond) \\ &= \left(s^2 + x^2 + y^2 + \frac{x^2y^2}{s^2}; \right. \\ &\qquad \left. 2sx + \frac{2xy^2}{s}, 2sy + \frac{2yx^2}{s}\right). \end{aligned} \tag{1}$$

To insure consistency, limits are always taken first on the director components and thereafter on the scalar component. For example, if $x = 0$ and $s = 0$, the limit on the director component $x \to 0$ is taken first $(s_\diamond; x_\diamond, y_\diamond) = (s^2 + y^2; 0, 2sy)$, and then the scalar limit $s \to 0$ is evaluated, thus $(s_\diamond; x_\diamond, y_\diamond) = (y^2; 0, 0)$. This criterion is actually extended to other functional relationships. The limit of scator components are taken in succession. For the present purposes, the order of *successive limits* is evaluated first for the director components in any order, and thereafter, the scalar component limit is evaluated.

The square of the magnitude of a scator $\|\overset{o}{\varphi}\|^2$ for a hyperbolic scator $\overset{o}{\varphi} = (s; x, y)$ is defined by

$$\|\overset{o}{\varphi}\|^2 = \left(s^2 - x^2 - y^2 + \frac{x^2y^2}{s^2}; 0, 0\right). \tag{2}$$

A scator with only nonvanishing first component is equal to a real scalar and can thus be used as an order parameter. This quantity is used to establish the bound criterion. The *conjugate* of a scator $\overset{o}{\varphi} = (s; x, y)$ is defined by the negative of the

[1] \overset{o} in LaTeX lore.

director components, while the scalar component remains unchanged $\overset{o}{\varphi}^* \equiv (s; -x, -y)$. The multiplicative inverse of $\overset{o}{\varphi}$ is

$$\overset{o}{\varphi}^{-1} = \frac{1}{s^2\left(1-\frac{x^2}{s^2}\right)\left(1-\frac{y^2}{s^2}\right)}\overset{o}{\varphi}^*. \tag{3}$$

From the above expression, $\overset{o}{\varphi}$ is invertible, provided that

$$s \neq \pm x, \quad s \neq \pm y, \quad \text{and} \quad s \neq 0 \quad \text{when } xy \neq 0. \tag{4}$$

The subspace $\mathbb{E}^{1+2} \subset \mathbb{R}^3$, where the scator magnitude is finite is defined by

$$\mathbb{E}^{1+2} = \{\overset{o}{\varphi} = (s; x, y) : s \neq 0 \text{ if } x, y \neq 0\}, \tag{5}$$

that is, the scalar component should not be zero if the two director components are finite. Let the extended set $\overline{\mathbb{E}}^{1+2}$ be defined in a similar fashion as the extended complex plane but adding one more dimension; That is, the *extended scator set*

$$\overline{\mathbb{E}}^{1+2} = \mathbb{E}^{1+2} \cup \{\overset{o}{\varphi} : \|\overset{o}{\varphi}\|^2 = \infty\} = \mathbb{R}^3 \cup \{\infty\}, \tag{6}$$

involves three dimensions and includes the point(s) at infinity. If s becomes very small while x, y are both different from zero, the magnitude of the scator, from the norm definition (2), becomes very large. There is then a set of points on the x, y plane whose magnitude approaches infinity

$$\mathbf{R}_s = \Big\{(s; x, y) \in \overline{\mathbb{E}}^{1+2} : x \neq 0, y \neq 0, \|(s; x, y)\| \xrightarrow[s\to 0]{} \infty\Big\}. \tag{7}$$

This set is depicted in Fig. 1.

Definition 2.1. The point $(s_0; x_0, y_0)$ has a *divergent vicinity* if there exists a set of points $(s_0 + \delta s; x_0 + \delta x, y_0 + \delta y)$ for infinitesimal δs, δx, $\delta y \in \mathbb{R}$, whose magnitude tends to infinity $\|(s_0 + \delta s; x_0 + \delta x, y_0 + \delta y)\| \to \infty$.

Therefore, the point $(0; 0, 0)$ has a divergent vicinity. Furthermore, all points with infinitesimal scalar and arbitrary director components $(\delta s; x, y)$ have a divergent vicinity. The only points within the x, y plane that can be (but are not necessarily) bounded for $s = 0$ are those lying on the axes lines $x = 0$ or $y = 0$. Points on these axes have a finite square magnitude given by $s^2 - y^2$ and $s^2 - x^2$,

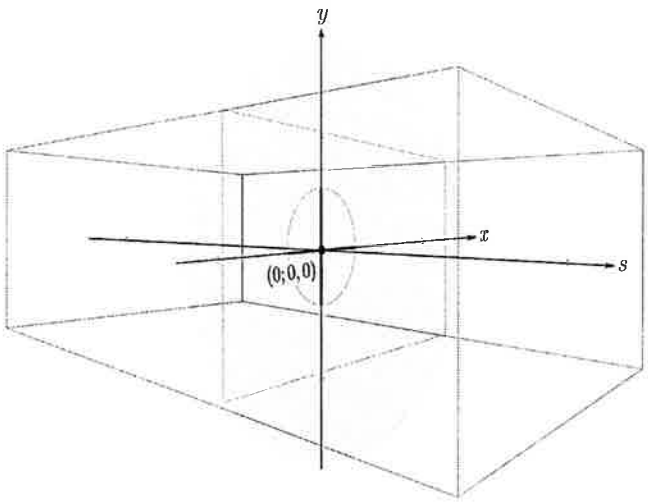

Fig. 1. Fixed point at the origin $0 = (0; 0, 0)$ and divergent magnitude plane (in gray) that covers the x, y plane except for the lines at $x = 0$ and $y = 0$. The darker cross in the x, y plane, whose length is $\pm 1/4$ in either axes, depicts the bound points on this plane under the quadratic iteration.

respectively. We discuss the on axis bound sets under the quadratic iteration in Sec. 4.1.

Let us now consider whether inverse orbits can be obtained within the scator number system in the quadratic mapping. There are two necessary conditions: (i) Elements have to be invertible under the addition and square operations, an essential property in order to evaluate the inverse mapping. (ii) Elements whose square is zero should be excluded, otherwise the inverse operation, i.e. square root of zero, could be undefined. Recall that the product of two nonzero scators can, in general, be zero. This assertion is often described as an algebra that contains divisors of zero. Consider the following two lemmas to establish the subset where the above conditions are fulfilled.

Lemma 1. *The square of an invertible element is also an invertible element.*

Proof. Consider an arbitrary invertible element, that is, an element $\overset{o}{\varphi} = (s; x, y)$ where $s^2 \neq x^2$, $s^2 \neq y^2$. The quotient of the director over scalar for the square operation is

$$\frac{x_\diamond}{s_\diamond} = \frac{2sx}{s^2 + x^2} = \frac{2\frac{x}{s}}{1 + \left(\frac{x}{s}\right)^2}, \quad \frac{y_\diamond}{s_\diamond} = \frac{2\frac{y}{s}}{1 + \left(\frac{y}{s}\right)^2}.$$

If any of these two components is noninvertible, the director and scalar component magnitudes have

to be equal. Consider, for example the x component $s_\diamond = \pm x_\diamond$. Then $1 + \left(\frac{x}{s}\right)^2 = \pm 2\frac{x}{s}$, that is $\left(\frac{x}{s} \pm 1\right)^2 = 0$. However, this condition can only be met if $s = \pm x$ but this equality contradicts the premise that the initial scator is invertible. A similar result follows for the y component. ■

Lemma 2. *There are no nilpotent elements in real scator algebra under the square operation.*

Proof. A scator element is zero if all its components are zero, i.e. $\overset{o}{\varphi} = 0 \Leftrightarrow \overset{o}{\varphi} = (0;0,0)$. An element is nilpotent if $\overset{o}{\varphi}^2 = (s_\diamond; x_\diamond, y_\diamond) = (0;0,0)$. For the square function (1), these conditions imply that $x^2 = -s^2$ and $y^2 = -s^2$. However, since s, x, y are real, these conditions are never attained. ■

Therefore, for all invertible initial points, preimages $O^-(\overset{o}{\varphi}_0)$ can be obtained under the quadratic mapping. Noninvertible points lie on planes defined by lines with slope equal plus or minus one in the s,x or s,y planes and arbitrary nonvanishing director component in the orthogonal direction. Namely, scator points with $x^2 = s^2$ for all $y \neq 0$, or $y^2 = s^2$ for all $x \neq 0$. Notice that the scalar component $s_\diamond$, resultant from the square operation (1), is always positive and different from zero for any nonzero scator since it is comprised by a sum of real square numbers.

3. Iterated Quadratic Mapping

The family of quadratic maps $P_c : z \mapsto z^2 + c$ from $\overline{\mathbb{E}}^{1+2}$ to $\overline{\mathbb{E}}^{1+2}$ is given by $\overset{o}{\varphi} = \overset{o}{\varphi}_0^2 + \overset{o}{c}$, where the variable $\overset{o}{\varphi}$ and the constant $\overset{o}{c}$ are now scator elements. The iterated function satisfies the recurrence relationship

$$\overset{o}{\varphi}_{n+1} = \overset{o}{\varphi}_n^2 + \overset{o}{c},$$

where the subindex stands for the iteration number. The Mandelbrot-like set is obtained by fixing the initial point $\overset{o}{\varphi}_0 = (0;0,0)$ and varying the parameter $\overset{o}{c}$. Bounded points obtained with this procedure comprise the corresponding M-set in $\overline{\mathbb{E}}^{1+2}$.

The confined M-like set in parameter space for real scators in $1+2$ dimensions is given by

$$\mathbf{S} = \{\overset{o}{c} \in \overline{\mathbb{E}}^{1+2} : n \in \mathbb{N}, \|P^{\circ n}(0)\| \nrightarrow \infty\},$$

where $P : \overset{o}{\varphi} \mapsto \overset{o}{\varphi}^2 + \overset{o}{c}$, $P^{\circ n}$ denotes the *n-fold composition* $P^{\circ n} = P \circ P \circ \cdots \circ P$ of the function P with itself and the 0 argument in $P^{\circ n}(0)$ means that the function is initially evaluated at zero. Some remarks are required: (i) the initial point in scator space $(0;0,0)$ is equal to the additive neutral $0 \in \mathbb{R}$; (ii) the **S** set has been defined by the set of points whose magnitude remains bounded. In complex algebra, it does not matter whether this condition is imposed on the magnitude or the real or imaginary parts. However, for real scators, these conditions are not equivalent just as it occurs for hyperbolic numbers [Pavlov *et al.*, 2009]; (iii) the M-set is alternatively defined by the set of parameters c for which K_c, the Julia set, is connected [Douady & Hubbard, 1984]. This approach will be deferred until the K_c set is discussed in a forthcoming communication.

In order to evaluate the points in the set numerically, it is more appropriate to cast the divergence condition in terms of an upper bound b

$$\mathbf{S} = \{\overset{o}{c} \in \overline{\mathbb{E}}^{1+2} : \forall n \in \mathbb{N}, \exists b \in \mathbb{R}, \|P^{\circ n}(0)\|^2 \leq b\}. \tag{8}$$

In real scator algebra, the magnitude squared is not positive definite. It is therefore necessary to perform the upper bound evaluation with the magnitude squared. For a different reason, namely, in order to avoid evaluating a CPU time consuming square root, it is customary to work with the square of the magnitude in the numerical code. The boundary of this set is contained in a three-dimensional space. In Fig. 2, the image of a three-dimensional rendering of the **S** set is shown. This and subsequent three-dimensional image representations were produced with Willenius rendering program [Willenius, 2013, v.2.0.1]. The number of points is 1.805×10^9, $(s = 1900) \times (x = 1900) \times (y = 500)$. Thirteen iterations are performed on each point. From these 1805 Mvoxels, only the points in the boundary are drawn. The coloring is due to the value of the components in the last iteration, the scalar, x and y directors' values are proportional to red, green and blue respectively $(s_{13}\{\text{red}\}; x_{13}\{\text{green}\}, y_{13}\{\text{blue}\})$. There is a bulge that looks smoother than the rest, spanning from 0 to 0.25 in the scalar axis (extreme right in Fig. 2). The confined set is squeezed at $s = 0$ where the bulge meets the complex structure on the left. The lack of bound points in the vicinity of the $s = 0$ plane is due to the divergent

Fig. 2. Three-dimensional rendering of the **S** set in $\overline{\mathbb{E}}^{1+2}$ $(s; x, y)$ viewed from the first director component, x axis. The abscissa corresponds to the real or scalar s axis ($-2.0 < s < 0.5$), while the ordinate depicts the second director component, y axis ($-1.2 < y < 1.2$). The x axis, coming out of the page, was scanned in the interval $-0.97 < x < 1.79$. 13 iterations per point were performed.

vicinity $\mathbf{R}_s$ described in (7). The rendering suggests a series of onion-like skins sewn at rather complex rims. Some of them resemble cardioid shapes while others do not seem to produce closed shapes. On the far left, there is a hint of a self-similar smaller version of the larger set. The entire fractal is inscribed in a diamond-like shape, that as we shall see, corresponds to the two-dimensional projection.

The **S** set in $\overline{\mathbb{E}}^{1+2}$ with axes labeled $(s; x, y)$ is drawn again in Fig. 3. However, the number of iterations for each point has been increased sevenfold from 13 (in Fig. 2) to 91. Since the bound set is defined for points where the magnitude remains bounded for an infinite number of iterations, it is expected that this latter rendering should be much closer to the actual set. This is true to some extent but it can be deceiving. Some regions in the set are extremely thin. When a few iterations are evaluated, these regions are partially "caught" within the bound criterion. However, as the number of iterations increases, if the mesh points do not intersect with the thin bound regions they become lost. To retain them, a much finer mesh is required with the concomitant increase in the number of operations. To grasp some of the finer details an incredibly thin mesh will be required. A possibility, in order to visualize these features, is to have a variable thickness evaluation mesh and to introduce transparency for very thin features.

3.1. *Self-similarity and symmetries*

To describe the main features of the 3D set, let us borrow the concept of "unit cell" or "elementary cell" from crystallography. The simplest repeating atomic distribution or structure in a crystal is called a unit cell or elementary cell.

Elementary fractal — Any of the subsets that contains the whole fractal structure that is repeated.

***n*th Elementary fractal** — The nth elementary fractal counted from large to small. The largest elementary fractal is labeled first, the second largest second, etc.

In Fig. 3, the first elementary fractal (first ef) spans from $(s; x, y)$ roughly equal to (-1.401 to 0.25; ± 1.125, ± 1.125). The second elementary fractal can just be resolved in this figure and is located around $(-1.769; 0, 0)$. Several other order elementary fractals have been observed along the negative

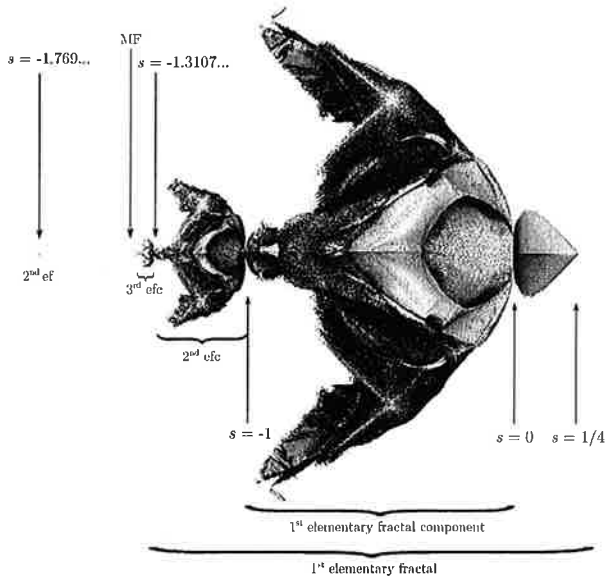

Fig. 3. Three-dimensional rendering of the **S** set in $\overline{\mathbb{E}}^{1+2}$ viewed from the first director component, x axis. 91 iterations per point were performed. The abscissa represents the real or scalar s axis, while the ordinate depicts the second director component, y axis.

s axis between -2 and -1.401. In crystallography, the elementary cell repeats with the same size and orientation producing a lattice. In three-dimensional fractals, the elementary fractal is repeated with the same shape but not necessarily with the same size nor orientation. In other words, the fractal lattice changes size and orientation. Furthermore, it need not be densely packed.

Elementary fractal component — A subset of the elementary fractal that is repeated within such structure. They are numbered from large to small.

There is an elementary fractal component contained within the volume given by (-1 to 0; ± 1.125, ± 1.125). The *first elementary fractal winged component* (first *efwc*). A second *efwc* is roughly located within (-1.3 to -1; $\pm 0.3, \pm 0.3$). These *efwc* are likely to be related to period-doubling regions. This period-doubling cascade seems to converge to the Myrberg–Feigenbaum (MF) point. These features are related to the bifurcation diagram of the logistic map in the next subsection. For $\overset{o}{c} = (s; x, y)$, the quadratic iteration recurrence relationship $\overset{o}{\varphi}_{n+1} = \overset{o}{\varphi}_n^2 + \overset{o}{c}$ for the scalar component is

$$s_{n+1} = s_n^2 + x_n^2 + y_n^2 + \frac{x_n^2 y_n^2}{s_n^2} + s \tag{9a}$$

and for the director components, the recurrence relationships are

$$x_{n+1} = 2 s_n x_n + \frac{2 x_n y_n^2}{s_n} + x, \tag{9b}$$

$$y_{n+1} = 2 s_n y_n + \frac{2 y_n x_n^2}{s_n} + y. \tag{9c}$$

Interchange of the x and y variables exchange the recurrence relationships for the director components. Thus, there should be symmetry with respect to the $\pm\pi/4$ axes in the x, y plane. This symmetry is clearly seen in Fig. 4, upper right and lower left insets, where the **S** set is seen from the $-s$ and $+s$ axes respectively.

In parameter space the initial point is $\overset{o}{\varphi}_0 = (0; 0, 0)$. The first iteration gives the iteration constant $\overset{o}{\varphi}_1 = \overset{o}{c} = (s; x, y)$. The second iteration for the scalar is

$$s_2 = s^2 + x^2 + y^2 + \frac{x^2 y^2}{s^2} + s \tag{10a}$$

and for the director components are

$$x_2 = 2x \left(s + \frac{y^2}{s} + \frac{1}{2} \right) \tag{10b}$$

$$y_2 = 2y \left(s + \frac{x^2}{s} + \frac{1}{2} \right). \tag{10c}$$

The x director component is an odd function of x, thus upon iteration, the function will be equal but with opposite sign under the transformation $x \to -x$. The bound criterion $\|\overset{o}{\varphi}\|^2 = \left(s^2 - x^2 - y^2 + \frac{x^2 y^2}{s^2}; 0, 0\right)$ is even under inversion of any of the axes. Therefore, the confined set and the escape velocity iso-surfaces must be symmetric about the ordinate axis. An equivalent reasoning leads to $y \to -y$ symmetry about the abscissas. The symmetry between the upper and lower halves in Fig. 4 exhibits this $\pm y$ symmetry. Renderings of rotations about the s axis (not shown here) also confirm the $\pm x$ symmetry. The bound set is asymmetrical with respect to the scalar (or real) s axis. Indeed, from the above expression, the transformation $s \to -s$ does not have a well defined parity for the resultant scalar term $s^2 + x^2 + y^2 + \frac{x^2 y^2}{s^2} + s$. Thus, the iterated map will not be equal under inversion of the scalar axis.

3.2. *Divergent magnitude set in the vicinity of periodic points*

Due to s terms in the denominators, all three components in iteration (10a)–(10c) become large for nonzero director components if the scalar becomes small. In a first approximation, allow for x, y to be small in the scalar component second iteration s_2, so that the term $\frac{x^2 y^2}{s^2}$ can be neglected; impose the condition $s_2 \to 0$, so that the scalar term will produce a very large scator in the third iteration. The equation for s_2 in terms of the initial values (10a) is approximately $s^2 + x^2 + y^2 + s = 0$. Notice that the s terms can be collected as $s^2 + s = \left(s + \frac{1}{2}\right)^2 - \frac{1}{4}$. The equation is then $\left(s + \frac{1}{2}\right)^2 + x^2 + y^2 = \frac{1}{4}$, that is a sphere of radius $\frac{1}{2}$ centered at $\left(-\frac{1}{2}; 0, 0\right)$. This sphere intersects the scalar axis at 0 and -1. Therefore, we expect to have an unbounded region in the vicinity of $s = -1$, as it is indeed observed in Fig. 3. Nonetheless, there is a period two fixed point at -1 with its concomitant basin of attraction. So there is an attractive point surrounded by divergent points on a plane. The surface generated

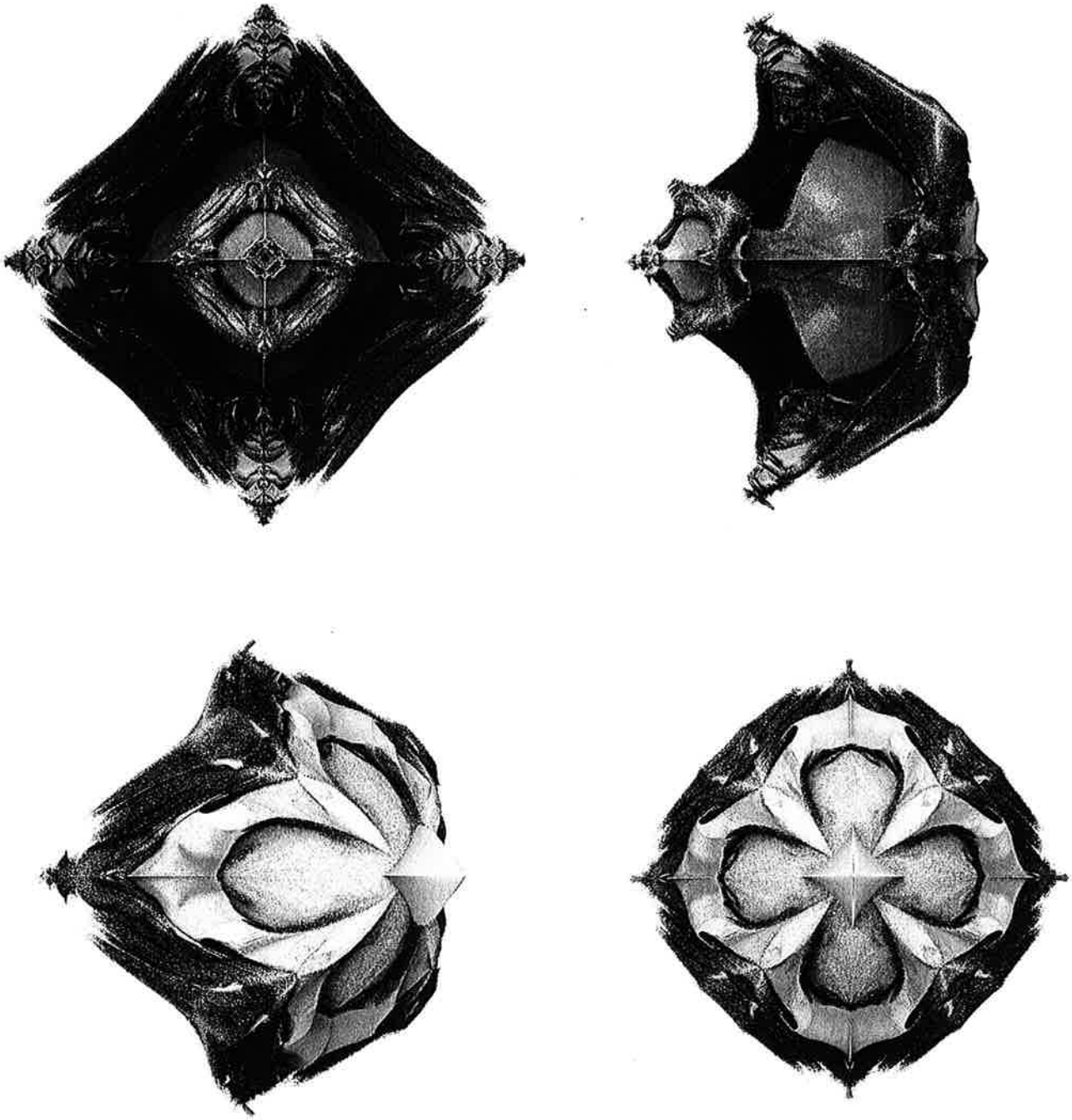

Fig. 4. Different views of the **S** set in $\overline{\mathbb{E}}^{1+2}$ seen from the (s, x) plane. The ordinates correspond to the y direction in all figures. Upper left: View from $-s$ axis. Upper right: View from $-\pi/4$ in (s, x) plane. Lower left: View from $\pi/4$ in (s, x) plane. Lower right: View from $+s$ axis. The x direction lies in the abscissa.

by the second iteration without approximations is $s^2 + x^2 + y^2 + \frac{x^2y^2}{s^2} + s = 0$, it is a slightly deformed sphere as shown in Fig. 5. This refinement does not alter significantly the argument that has been presented. We previously found a set of divergent magnitude points $\mathbf{R}_s$ in the vicinity of $(0; 0, 0)$. We have now found that there is also a divergent magnitude surface crossing the s axis at $s = -1$. Let us generalize this result.

Proposition 1. *For every periodic scator point on the scalar axis* $(s_n; 0, 0)$ *under the quadratic iteration mapping from* $\overline{\mathbb{E}}^{1+2}$ *to* $\overline{\mathbb{E}}^{1+2}$ *in parameter space,*

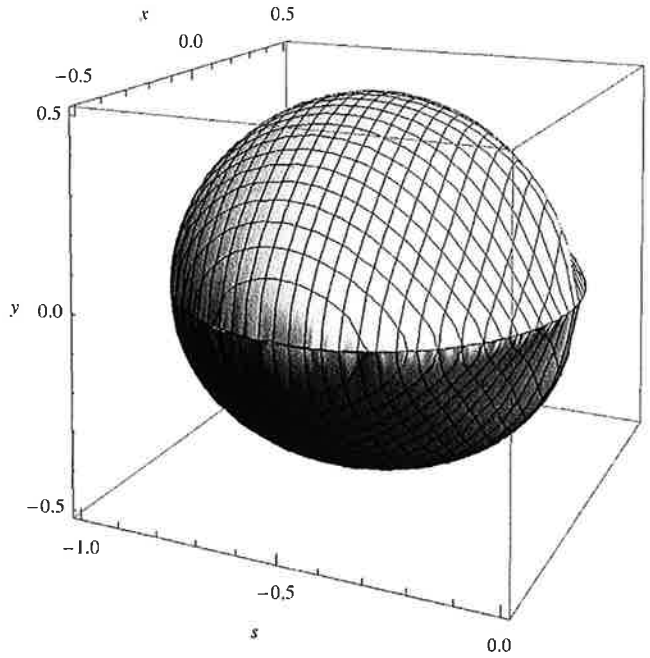

(a)

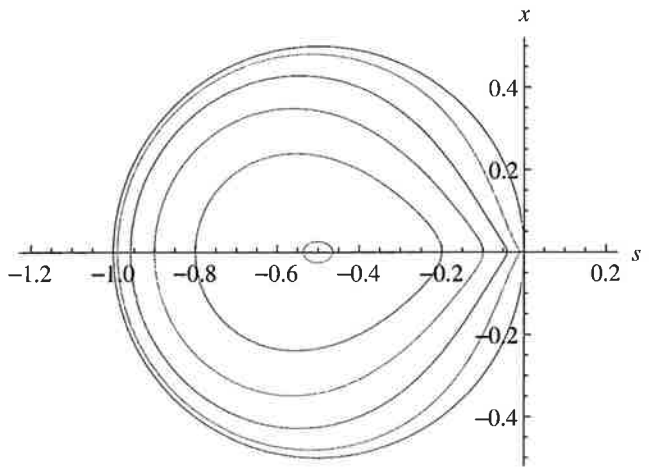

(b)

Fig. 5. Plot of equation $s^2 + x^2 + y^2 + \frac{x^2y^2}{s^2} + s = 0$. Along this surface, the scalar component in the second iteration is zero $s_2 = 0$. The scator magnitude diverges on this surface except at the planes $x = 0$ and $y = 0$. There is a period 2 point at $(-1; 0, 0)$ and the fixed point at the origin. (a) 3D rendering and (b) constant y curves for $y = 0$ (circle radius $1/2$ centered at $-1/2$), $y = 0.1, 0.2, 0.3, 0.4$ and 0.4987 (tiny curve centered at $-1/2$).

there is a divergent vicinity

$$\mathbf{R}_{s_n} = \{(s_n; x_n, y_n) \in \overline{\mathbb{E}}^{1+2} : x_n \neq 0, y_n \neq 0, s_n \to 0\}.$$

Proof. On the one hand, a divergent magnitude is obtained when the scalar component of the nth iteration scator is zero, while the director components remain finite. That is, $\|\overset{o}{\varphi}_n\| = s_n^2 - x_n^2 - y_n^2 + \frac{x_n^2 y_n^2}{s_n^2} \to \infty$ if $s_n(s, x, y) \to 0$, while $x_n(s, x, y) \neq 0$ and $y_n(s, x, y) \neq 0$. Notice that if the director components are not zero after n iterations, they are necessarily nonzero for the initial constant value $\overset{o}{c} = (s; x, y)$, that is $x_n, y_n \neq 0 \Rightarrow x, y \neq 0$. On the other hand, periodic points with period n require that $\overset{o}{\varphi}_n = 0$, that is, the point represented by the scator $\overset{o}{\varphi}$ returns to zero after n iterations. Since x, y are zero on the scalar axis, $\overset{o}{\varphi}_n = (s_n; 0, 0) = 0$ for periodic points on the scalar axis. But a scator with zero director components is equal to a scalar, i.e. $(s_n; 0, 0) = s_n$. Furthermore, on the scalar axis, s_n is only a function of s, namely $s_n(s, 0, 0) = 0$. But this periodic point condition on the scalar axis is equal to the divergent magnitude limit $s_n(s, x, y) \to 0$ if $x = y = 0$. The on axis periodic point $(s_n; 0, 0)$, has a divergent vicinity, for there exists a set of points $(s_n; \delta x_n, \delta y_n)$ with infinitesimal $\delta x_n, \delta y_n$, whose magnitude diverges since $s_n(s, \delta x, \delta y) = 0$ while $\delta x_n, \delta y_n$ are different from zero. ■

Thus the divergent magnitude surface defined by the polynomial $s_n(s, x, y) = 0$ has a periodic point whenever it intersects the scalar axis. The iterations on the scalar or real axis commence with the constant $\overset{o}{c} = (s; 0, 0)$. From (1), the square of a scator with zero director components is a scator whose only nonvanishing component is again the scalar component. Recall also, that addition is defined component-wise. Thus the iteration of a scalar quantity remains a scalar. In this particular case, the zeros in the director components $(s; 0, 0)$ can be dropped and only the real number s need be written down. The real roots of the corresponding polynomials establish the periodic points after n iterations. The second column in Table 1, shows the well known first few roots on the real line [Alligood *et al.*, 2000]. There are basins of attraction in the vicinity of these attractive periodic points in the complex plane. We assume without proof, that there are also basins of attraction in the three-dimensional real scator space. This assumption is consistent with the numerical evaluation that exhibits smaller 3D copies of the set at the roots of the polynomial in the negative real axis (see Figs. 2 and 3).

Table 1. Attractive periodic points on scalar axis and divergent magnitude surfaces due to scalar component equal to zero.

Point Period	Periodic Points on Scalar Axis $\overset{o}{\varphi}_n = 0$	Real Root	Divergent Scator Magnitude $s_n = 0$
Initial value	$x, y = 0$		$x, y \neq 0$
Fixed	$\overset{o}{\varphi}_1 = s$	$s = 0$	$s_1 = s$
2	$\overset{o}{\varphi}_2 = s^2 + s$	$s = -1$	$s_2 = s^2 + x^2 + y^2 + \frac{x^2 y^2}{s^2} + s$
3	$\overset{o}{\varphi}_3 = (s^2 + s)^2 + s$	$s = -1.7549$	$s_3 = s_2^2 + x_2^2 + y_2^2 + \frac{x_2^2 y_2^2}{s_2^2} + s$
4	$\overset{o}{\varphi}_4 = ((s^2 + s)^2 + s)^2 + s$	$s = -1.3107$	$\vdots$

On the other hand, points in the vicinity of the divergent magnitude surface with $s_n \ll x_n, y_n$, will have a large magnitude and will fail to fulfill the upper bound criterion (8). Furthermore, all three components in the $n+1$ iteration (9a)–(9c) become large for nonzero director components if the s_n scalar becomes very small. Imposing the condition that the scalar component becomes zero in the nth iteration, produces a divergent result for all three components in the next iteration if $x_{n+1}, y_{n+1} \neq 0$. In contrast with what we stated before, in this case, the large magnitude condition is equivalent to the large scalar component condition. The corresponding polynomials are shown in the last column of Table 1. These polynomials involve three variables and thus establish a two-dimensional surface embedded in a three-dimensional space.

The basin of attraction of periodic points on the scalar axis becomes squeezed in the x, y plane at the periodic point. This is indeed what is observed in Fig. 3. The roots at 0, -1, -1.3107 clearly exhibit a waist. Recall that the logistic map exhibits a one-to-one correspondence with the M-set real axis intersection. The Mandelbrot period doubling bulbs meet at the bifurcation points. The center of the bulbs correspond to the super-stable periodic points. The **S** set in $\overline{\mathbb{E}}^{1+2}$ exhibits the same one-to-one correspondence with the bifurcation diagram of the logistic map $z \mapsto \lambda z(1-z), z \in \mathbb{R}$ on the scalar axis since the quadratic iteration is identical for complex, hyperbolic or scator numbers that lie on the real axis. Off the scalar axis, the periodic points show a waist due to the divergent vicinity as we have just shown. Therefore, there is a one-to-one correspondence of these waists of the **S** set in $\overline{\mathbb{E}}^{1+2}$ with the values in each periodic window centered in the middle between bifurcations of the Verhulst process.

The nature of the basin of attraction of periodic orbits of continuous maps on the real line has great importance. There are no globally attractive periodic orbits of continuous maps on connected metric spaces. In contrast, fixed points can be globally attractive [Elaydi & Sacker, 2004]. It will be interesting to attempt extending the dynamics in the neighborhood of a periodic point to higher dimensions such as three-dimensional scators.

The extended complex plane is homeomorphic to the two-dimensional sphere $S^2 = \{(x_1, x_2, x_3) \in \mathbb{R}^3 : x_1^2 + x_2^2 + x_3^2 = 1\}$. Infinity in $\overline{\mathbb{C}}$ is then mapped onto a single point at the sphere pole $x_3^2 = 1$. The point at infinity can then be thought as a super-attractive fixed point [Blanchard, 1984]. Whether it is possible to produce a homeomorphism of $\overline{\mathbb{E}}_{-}^{1+2}$ with a three-dimensional sphere embedded in four dimensions is an open problem. Nonetheless, we can anticipate that the scator divergent magnitude surface can be thought as a super-attractive surface at infinity.

4. Sections of the S Set in the s, x Plane

4.1. *Quadratic iteration with hyperbolic numbers*

In $1+1$ dimensions, positive or real scator algebra becomes identical to hyperbolic numbers algebra $\mathbb{H}$. Furthermore, distributivity of the product over addition is recovered. Since hyperbolic numbers are equivalent to scators with only one director component $\mathbb{H} \to \mathbb{E}^{1+1}$, the M-set in $\mathbb{H}$ and **S** in $\mathbb{E}^{1+1}$

are equal. The quadratic iteration with hyperbolic numbers gives rise to a square centered at $-\frac{7}{8}$ with sides equal to $\frac{9}{4\sqrt{2}}$ [Senn, 1990]. The square diagonals (with $\frac{9}{4}$ length) lie parallel to the real and hypercomplex axes. If the bound criterion for a hyperbolic number $a + b\hat{\mathbf{e}}$, $(\hat{\mathbf{e}} \cdot \hat{\mathbf{e}} = 1, \hat{\mathbf{e}} \notin \mathbb{R})$ is $a^2 \leq \varepsilon$ and $b^2 \leq \varepsilon$, the bound set is equal to a square [Metzler, 1994]. This set is the counterpart of the Mandelbrot set for complex numbers but in two-dimensional hyperbolic geometry [Artzy, 1992]. The boundary for the hyperbolic set, is made up of four straight lines void of the complexity shown by the M-set. There are neither small-copies of the set nor a structure within the bound region as can be seen in the first upper left inset of Fig. 6. Thus, the rich fractal 3D structure is lost when it is projected into 2D.

The iteration on the real positive axis is bound from 0 to 1/4. The iteration on the director axes for $s = 0$ is also bound from 0 to 1/4 since the sides of the square bound set are rotated at $\pi/4$. Since the mapping is symmetric with respect to the director axes it must be bound from $-1/4$ to 1/4. A similar argument follows for the other director axis. So the points located within a cross centered at the origin of the x, y plane at $s = 0$ with 1/4 length per arm produce bound iterations. The quadratic iterated function of any other point in the $s = 0$ plane diverges as shown in Fig. 1.

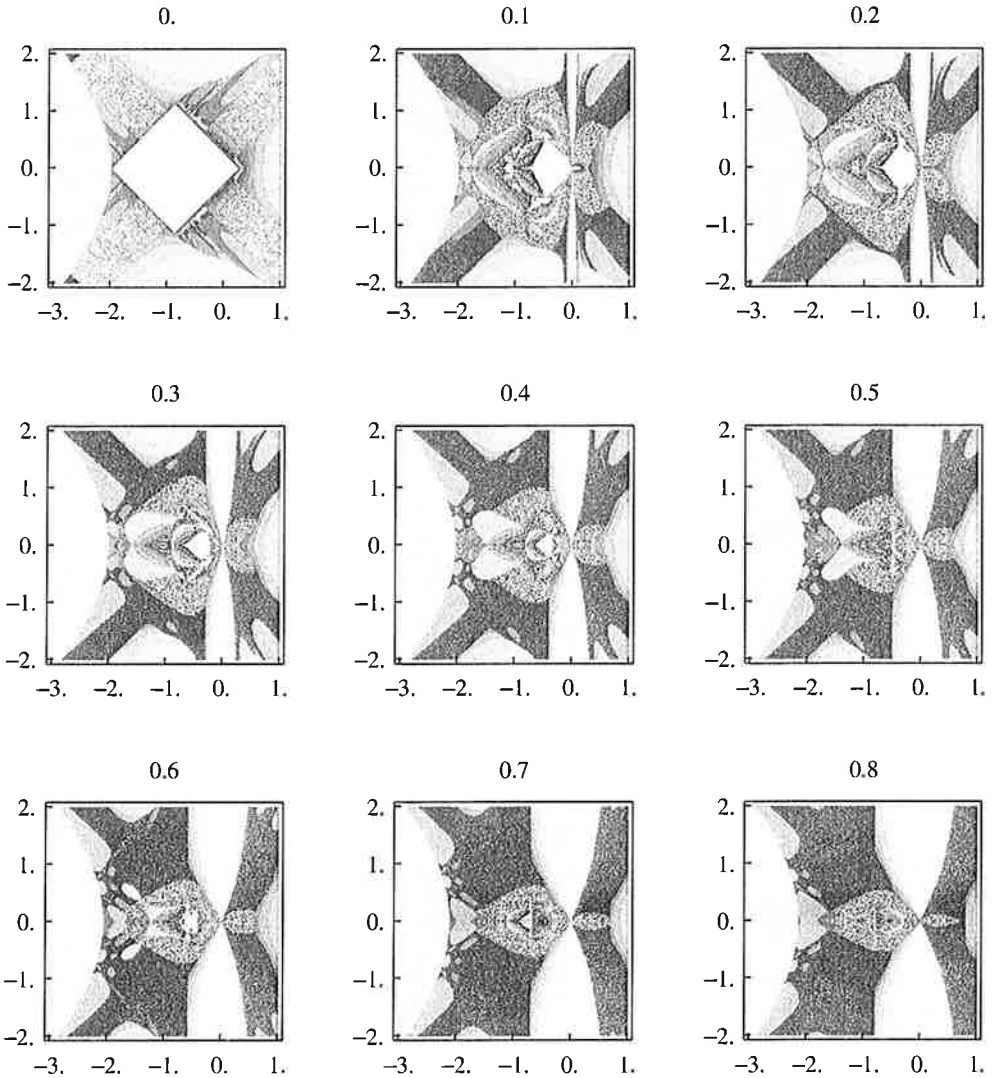

Fig. 6. Slices of the bound quadratic iteration $\mathbf{S}\ (s; x, y)$ set at constant y hyperaxis between 0 and 0.8 in 0.1 steps. The abscissa s is scanned in the ± 2.0 interval centered at -1.0 whereas the ordinate x is scanned in the same interval but centered at the origin.

4.2. *The s, x plane*

There are an arbitrary number of intersections of the plane with a volume depending on the position and inclination of the plane. Therefore, there are infinitely many slices of the M-like set in $\overline{\mathbb{E}}^{1+2}$ compared with the unique set obtained in $\mathbb{C}$. A rich fractal-like structure is revealed if the second director component is set to small value different from zero. Evaluation at hypercomplex plane $y = 10^{-20}$ already exhibits a complex structure [Fernández-Guasti, 2013]. In a sequence, depicted in Fig. 6, we show projections of $\mathbf{S}$ in $\overline{\mathbb{E}}^{1+2}$ from $(s; x, 0)$ to $(s; y, 0.8)$ in steps of $\triangle y = 0.1$. Points are evaluated starting at $\overset{o}{\varphi}_0 = (0; 0, 0)$ and $\overset{o}{c} = (s; x, y)$, s is scanned in the ± 2.0 interval centered at -1.0 while x is centered at 0. The bounded region becomes smaller and departs form the diamond-like shape moving towards a bird-like form as the y hyperplane is increased. The set is always squeezed in the forefront to the right in the plane where $s = 0$ if $y \neq 0$. Furthermore, the escape velocity in the $s = 0$ plane is very large (lighter blue) as may be seen in the insets of Fig. 6. This plane is enlarged as the y plane is further away from the origin. This is the expected behavior due to the large magnitude set $\mathbf{R}_s$ described in (7) encountered in the vicinity of the $s = 0$ plane. A large escape velocity (light blue) circle with radius approximately $1/2$ centered around $s = -1/2$ can be clearly seen in the insets $y = 0.1$ and 0.2 of Fig. 6. These large iso-escape velocities correspond to the second iteration divergent magnitude surface $s_2 = s^2 + x^2 + y^2 + \frac{x^2y^2}{s^2} + s = 0$. The level curves plotted in Fig. 5 can be followed in the insets 0.1 to 0.4 of Fig. 6. At $y = 0.5$, the second iteration divergent magnitude surface just touches the plane at only one point and is no longer present for $y > 0.5$.

So far, we have described squeezing of the set at the periodic points on the scalar axis. The $\mathbf{R}_{s_2}$ surface also prevents points to be bounded off axis. The bound set is squeezed when it meets the rim of the $\mathbf{R}_{s_2}$ surface. See for example the thin attachment of the wings to the main body in insets 0.1 to 0.4 of Fig. 6. The $\mathbf{R}_{s_2}$ surface attracts points that approach it, since the $n+1$ iteration will have very large values for all three components.

The $s_3 = 0$ polynomial is already rather lengthy to write down in terms of the initial $\overset{o}{c} = (s; x, y)$ values. Its roots are analytically solvable although they are even lengthier. However, the intersection of this surface with the $y = 0$ plane is quite tractable. From Table 1,

$$s_3 = s_2^2 + x_2^2 + s,$$

because $y = 0 \Rightarrow y_2 = 0$. Substitution of s_2 and x_2 from (10a) and (10b) respectively gives

$$s_3 = (s^2 + x^2 + s)^2 + 4x^2\left(s + \frac{1}{2}\right)^2 + s = 0.$$

The real solutions for x are

$$x = \pm\frac{\sqrt{\sqrt{32s^4 + 64s^3 + 44s^2 + 8s + 1} - (6s^2 + 6s + 1)}}{\sqrt{2}},$$

this function is plotted in Fig. 7. The magnitude squared for a scator in the third iteration is

$$\|\overset{o}{\varphi}_3\|^2 = s_3^2 - x_3^2 - y_3^2 + \frac{x_3^2 y_3^2}{s_3^2}.$$

Since $y = 0 \Rightarrow y_3 = 0$, then $\|\overset{o}{\varphi}_3\|^2 = s_3^2 - x_3^2$ and for points on the intersection with the surface $s_3 = 0$

$$\begin{aligned}\|\overset{o}{\varphi}_3\|^2 &= -x_3^2 = -(2s_2x_2 + x)^2 \\ &= -(2x(s^2 + x^2 + s)(2s + 1) + x)^2,\end{aligned}$$

where we have used the iteration relationship (9b). This magnitude is certainly finite in the interval ± 2 in either variable. However, as soon as $y \neq 0$, the magnitude becomes divergent. The curve shape is not altered significantly for very small values of y. Just as in the $s_2 = 0$ condition, small departures from $y = 0$ yield similar curves, as observed in Fig. 5. There is a high escape velocity (light blue) contour of the form given by the $s_3 = 0$ polynomial (depicted in Fig. 7) in inset 0.1 of Fig. 6. Again, at approximately $s = -0.9, x = \pm 0.9$ the confined set is squeezed due to the presence of the third iteration divergent magnitude surface. The out-most bound point must be located at $y = \frac{9}{8} = 1.125$ where the upper tip of the diamond is located. Recall that there must be a diamond-like shape in the perpendicular s, y plane identical to the one shown in the first s, x inset. This feature is no longer visible even at smaller values of the y planes because the tip

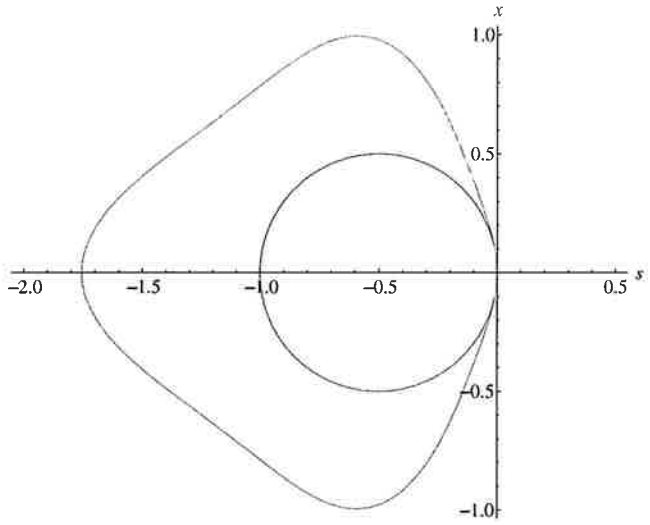

Fig. 7. Intersection of the $s_3 = 0$ and $s_2 = 0$ (circle) surfaces with the $y = 0$ plane.

becomes very thin and is difficult to see at this magnification. From previous estimates [Fernández-Guasti, 2013], the tip is approximately 10^{-7} thick between 1.0 and 1.125.

Now that we have an explicit negative square magnitude in the above equation, let us comment on this issue. The square of the scator magnitude is not positive definite as may be seen from its definition (2). However, when comparing with the bailout number b, it makes no difference if the absolute value of the square magnitude is considered in the numerical evaluation or not. This somewhat baffling result can be explained as follows. The magnitude is negative if one of the two director components is larger than the scalar component. Take for example, the point $(0; x_3, 0)$, whose magnitude squared is negative $\|(0; x_3, 0)\|^2 = -x_3^2$. However, notice that in the next iteration, the square of this number needs to be taken. From the squaring operation definition $(0; x_3, 0)^2 = (x_3^2; 0, 0)$, that is, the director components become zero and the scalar component is nonvanishing. The square magnitude of this scator then becomes positive $\|(x_3^2; 0, 0)\|^2 = x_3^4$. Therefore, the squaring operation within the iteration procedure, prevents a negative square magnitude from growing towards negative values indefinitely.

5. Conclusions

The **S** set in $\overline{\mathbb{E}}^{1+2}(s; x, y)$ has been defined in parameter space in terms of bounded iterations under the quadratic mapping. The salient feature is that the three-dimensional set exhibits a rich fractal boundary whereas the two-dimensional projection has a smooth nonfractal boundary. For this reason, the fractal structure is intrinsically three-dimensional. Some features of the 3D set have been described, such as the self-similarity of the elementary fractal as well as elementary fractal components. The position of self-similar smaller copies near the scalar axis coincide with their counterparts in the Mandelbrot set [Fernández-Guasti, 2013]. The elementary fractal components exhibit a one-to-one correspondence with the bifurcation diagram of the logistic map on the scalar axis.

The extended scator set $\overline{\mathbb{E}}^{1+2}$ that includes the points at infinity has been introduced. Besides the usual points whose components tend to infinity, this set also contains scator elements with null scalar and finite director components. It has been shown that inverse orbits can be obtained for all invertible points in $\overline{\mathbb{E}}^{1+2}$. Although scator algebra contains divisors of zero, these products do not interfere with inverse orbits since there are no nilpotent elements under the square operation.

The main proposition establishes that for every periodic point on the scalar axis there exists a divergent vicinity. In the vicinity of the scalar axis, the periodic points show a waist centered in the middle between bifurcations due to the concomitant divergent neighborhood. Squeezing of the set at the divergent magnitude surfaces has also been observed off the scalar axis. However, only the divergent vicinity for the on axis periodic points has been proved here. There is no counterpart to this periodic point — divergent vicinity behavior in the M-set.

The principal symmetries of the **S** set have been discussed. Most important is the symmetry between the two director hypercomplex axes. In contrast, recall that other algebraic generalizations to higher dimensions do not exhibit identical properties when hypercomplex components are interchanged. Images of the three-dimensional boundary of this set have been rendered with the open source program developed by Willenius [2013]. We have shown that increasing the number of iterations gives a closer fidelity to the actual set boundary but some features are lost. In particular, very thin surfaces are no longer rendered. A possibility in order to visualize these features is to have a variable thickness evaluation mesh and to introduce transparency for very thin features. New algorithms will certainly be required to visualize the intricacies of these higher

dimensional sets. Two-dimensional renderings also prove useful to understand the dynamics. In particular, they have been utilized here in order to assess escape velocities that are related to the $\mathbf{R}_{s_n}$ divergent magnitude surfaces.

Acknowledgments

I am greatly indebted to A. Vilchis, F. Zaldívar and J. L. del Río for their critical reading of the early scator algebra manuscripts.

References

Alligood, K. T., Sauer, T. & Yorke, J. A. [2000] *Chaos: An Introduction to Dynamical Systems*, 3rd edition (Springer-Verlag).

Artzy, R. [1992] "Dynamics of quadratic functions in cycle planes," *J. Geom.* **44**, 26–32.

Blackledge, J. [2002] *Fractal Geometry: Mathematical Methods, Algorithms, Applications* (Woodhead Publishing).

Blanchard, P. [1984] "Complex analytical dynamics on the Riemann sphere," *Am. Math. Soc.* **11**, 85–141.

Dodge, M., McDerby, M. & Turner, M. J. (eds.) [2008] *Geographic Visualization: Concepts, Tools and Applications* (Wiley-Blackwell).

Douady, A. & Hubbard, J. H. [1984] "Exploring the Mandelbrot set," Tech. rep., Université Paris Sud.

Elaydi, S. & Sacker, R. [2004] "Basin of attraction of periodic orbits of maps on the real line," *J. Diff. Eqs. Appl.* **10**, 881–888.

Fernández-Guasti, M. [2013] "Fractals with hyperbolic scators in $1 + 2$ dimensions," *Fractals*, submitted.

Fernández-Guasti, M. & Zaldívar, F. [2013] "A hyperbolic nondistributive algebra in $1 + 2$ dimensions," *Adv. Appl. Clifford Algebr.* **23**, 639–653.

Helmstetter, J. & Micali, A. [2008] *Quadratic Mappings and Clifford Algebras* (Birkhäuser Basel).

Kantor, I. L. & Solodovnikov, A. S. [1989] *Hypercomplex Numbers* (Springer-Verlag), translated by A. Shenitzer.

Leys, J. [2005] "Sphere inversion fractals," *Comput. Graph.* **29**, 463–466.

Metzler, W. [1994] "The 'mystery' of the quadratic Mandelbrot set," *Am. J. Phys.* **62**, 813–814.

Pavlov, D. G., Panchelyuga, M. S., Malykhin, V. A. & Panchelyuga, V. A. [2009] "On fractality of Mandelbrot and Julia sets on double-numbers plane," *Hypercompl. Numbers in Geom. Phys.* **6**, 135–145.

Rama, B. & Mishra, J. [2011] "Generation of 3D fractal images for Mandelbrot set," *Proc. 2011 Int. Conf. Communication, Computing & Security*, ICCCS '11 (ACM, NY, USA), pp. 235–238.

Sabadini, I., Shapiro, M. & Sommen, F. (eds.) [2009] *Hypercomplex Analysis*, Trends in Mathematics (Birkhäuser).

Senn, P. [1990] "The Mandelbrot set for binary numbers," *Am. J. Phys.* **58**, 1018.

Willenius, P. [2013] "Fractrace," URL https://github.com/trafassel/Gestaltlupe.